Available online at www.sciencedirect.com
SCIENCE DIRECT®
Computerized Medical Imaging and Graphics 27 (2003) 503–512
Computerized Medical Imaging and Graphics
www.elsevier.com/locate/compmedimag

Snake modeling and distance transform approach to vascular centerline extraction and quantification

Mahnaz Maddah[a,b], Hamid Soltanian-Zadeh[a,b,c,*], Ali Afzali-Kusha[a]

[a]*Control and Intelligent Processing Group, Department of Electrical and Computer Engineering, University of Tehran, Tehran, Iran*
[b]*Signal and Image Processing Group, School of Intelligent Systems, Institute for Studies in Theoretical Physics and Mathematics, Tehran, Iran*
[c]*Image Analysis Laboratory, Department of Radiology, Henry Ford Health System, One Ford Place, 2F, Detroit, MI 48202, USA*

Received 4 October 2002; revised 14 April 2003; accepted 14 April 2003

Abstract

A new method for fully automated centerline extraction and quantification of microvascular structures in confocal microscopy (CM) images is presented. Our method uses the idea of active contour models as well as path planning and distance transforms for the three-dimensional centerline extraction of elongated objects such as vessels. The proposed approach is especially efficient for centerline extraction of complex branching structures. The method performance is validated in several CM images of both normal and stroked rat brains as well as simulated objects. The results confirm the efficiency of the proposed method in extracting the medial curve of vessels, which is essential for the computation of quantitative parameters.

Keywords: Active contour models; Centerline extraction; Vascular quantification; Confocal microscopy

1. Introduction

Numerous three-dimensional (3D) visualization tools exist to process and visualize thin 3D structures such as vessels. The most common tool is maximum intensity projection (MIP), which is a very simple ray tracer [1]. It generates a 2D projection of 3D object along a single direction, leading to some drawbacks such as visual occultation of vessels and artificial crossings that can only be detected by matching on several other projections [1]. Also, quantitative parameters such as diameter, length and volume of vessels, which are beneficial for diagnosis, planning surgery and therapy, are not accurately estimated. So, an accurate processing of the 3D images is required for a reliable visualization and proper extraction of the vessel parameters. Obtaining the 3D main structure or the centerline of the objects has received a great attention in recent years for its applications in data compression, medical image analysis, path planning, etc. Moreover, centerline extraction is the first and the most important step for quantification of tubular objects such as vessels. A number of methods for 3D skeletonization or centerline extraction of objects have been introduced in recent years, which are mostly extensions of 2D methods.

The most popular methods for skeletonization are distance transform (DT)-based techniques [2–7], which tend to determine medial points by locating voxels lying farthest with respect to the boundary of the object on its cross-section normal to the local major axis. The method was first introduced by Blum [2], in which the DT of object voxels with respect to boundary voxels was used to determine maximal balls (disks) within a 3D (2D) object. The maximal balls are sphere-like sets of connected voxels with maximum radius, which are completely contained in the object but not in any other ball in the object. It has been shown that any object can be fully represented by the set of its maximal balls [3], whose set of centers gives the skeletal voxels.

Thinning methods are another category of skeletonization [8–12]. The idea is to apply morphological erosion operators to successively 'peel off' the outer layer of the object until it is reduced to its skeleton. To prevent

* Corresponding author. Address: Image Analysis Laboratory, Department of Radiology, Henry Ford Health System, One Ford Place, 2F, Detroit, MI 48202, USA. Tel.: +1-313-874-4482; fax: +1-313-874-4494.
E-mail address: hamids@rad.hfh.edu (H. Soltanian-Zadeh).

0895-6111/03/$ - see front matter © 2003 Elsevier Ltd. All rights reserved.
doi:10.1016/S0895-6111(03)00040-5

over-thinning of the object, the deletion of the object end-points should be avoided and only boundary voxels whose removals do not affect the connectivity and structural topology should be removed. Most of the proposed 3D thinning methods extract the medial surface of the object where other algorithms are needed to obtain the medial curve from the medial surface [10,13]. These methods are generally faster than the DT-based methods, but the extracted skeleton might contain extra or missing skeleton branches.

Another type of centerline extraction technique is called the path planning method [14–16], which has applications in virtual endoscopies and robotic path planning. The idea is to choose an initial path along the object, connecting two given points. The path is then adjusted toward the central axis.

A major drawback of all these methods is that the user must define the start- and end-points of the paths. This is a very tedious and almost impossible task when dealing with complex and branching structures like vessels. In our previous work [17,18], we automated the end-point identification using a distance map and applied it for centerline extraction of vascular structures.

Some other works have focused only on vessel detection and quantification [19], where a multi-scale approach with a Gaussian modeling of the intensity profile inside the vessels is used. The convolution of the image with a series of Gaussian kernels with different standard deviations gives a scale-set of images where centerlines are detected as local extremes of a response function, designed for a set of models [20,21]. In another work [22], the authors estimated the centerline after segmenting the image by skeletonization. These works use convolutions with several Gaussian kernels and thus are time-consuming. The skeletonization methods based on fuzzy theory [23], neural networks [24], and generalized potential field [25], are also very slow, though they produce accurate and reconstructable skeletons.

For quantification of vessels, a 3D skeletonization approach should be time efficient for processing a large real dataset and fully automated for the centerline extraction of any branching structure. The extracted skeletons should be accurately centered with distinguishable parts and a thin connected centerline.

In this paper, we present a novel method for fast and accurate extraction of centerlines of 3D elongated objects with the desired features mentioned earlier. The method can be effectively applied to the complex branching structures in vascular images. The extraction process does not require any user interaction or prior knowledge of the object shape. We have applied this method to several confocal microscopy (CM) datasets to evaluate the results. However, the technique is general and can be applied to other 3D image datasets for centerline extraction. In Section 2, the proposed algorithm is presented, while the improvements to the method are described in Section 3. In Section 4, the experiments and results are given and finally summary and conclusions are given in Section 5.

2. Proposed centerline extraction algorithm

The goal is to extract a 3D centerline of any branching object, hence the first step is to distinguish the different branches of the structure. In doing so, we invoke the method proposed in our previous work [17], to identify the end-points of branches using a distance map from a predefined reference point (RP). Next, a set of 26-neighbor voxels called paths, connects each end-point to the RP [14]. A voxel path connecting voxels V_1 and V_n is defined as an ordered sequence of voxels, $\{V_1, V_2, \ldots, V_{n-1}, V_n\}$ such that any two voxels V_i and V_{i+1} have 26-connectivity. Each voxel in the path is associated with its cumulative distance back to the start voxel along the polyline connecting the centers of path voxels in sequence [14]. Now the issue is to move these paths toward the centerline of the object. For this purpose, we employ a variant of the snake model, introduced by Kass [26], where the paths are considered as snakes. The snakes are evolved in order to minimize the image potential energy, which is defined here as the gradient of the computed distance map, as defined below, from the boundary of the object. Forces are applied to the snakes to shift them in the direction of decreasing the gradient. After a few iteration, the snakes will be located at the center of the object where the gradient field has its minimum value, which is usually zero. During the translation of the voxels of the snakes, the voxels might overlap with or get far from each other. To obtain connected and fine paths as the centerlines of the object, an up–down sampling on the final snakes is performed. In the following, different stages of the approach are described in detail.

2.1. Segmentation and surface extraction

After performing the required preprocessing tasks such as filtering and thresholding as will be mentioned in Section 4, a binary structure of interest is segmented using a region-growing algorithm [4]. The seed voxel for region growing is the first foreground voxel met in scanning the image sections. A region of 26-connected voxels is then grown outward. The last voxel marked, is chosen as the Start Point (SP) and also as the RP for the DT mapping. Having the object segmented, the boundary surface, which is needed for both gradient field construction and paths initialization, is extracted.

2.2. Energy and gradient field construction

Using the object surface, the distance to the boundary is computed using a front propagation procedure [4]. Performing the front propagation procedure on all voxels of

the extracted surface, we compute the distance map, denoted D, visiting only the voxels inside the object. For all the voxels outside the object $D(i,j,k)$ is assumed -1 and for all voxels on the surface, $D(i,j,k)$ is considered zero. The value of D is increased for the central voxels as shown in Fig. 1(a).

Interpreting the distance map D as a discrete 3D scalar field, one can easily compute its approximate gradient for a grid point by building finite differences in each of directions i, j and k of the scalar field [6]:

$$G(i,j,k) = \nabla D(i,j,k) = \begin{pmatrix} 0.5(D(i+1,j,k) - D(i-1,j,k)) \\ 0.5(D(i,j+1,k) - D(i,j-1,k)) \\ 0.5(D(i,j,k+1) - D(i,j,k-1)) \end{pmatrix} = \begin{pmatrix} G_x \\ G_y \\ G_z \end{pmatrix} \quad (1)$$

G is the gradient vector with the components of G_x, G_y and G_z, respectively, in the directions of x, y and z. The result of the discrete gradient computation is a 3D vector field. In order to obtain a continuous gradient function in 3D space, the gradient at the point $(x+a, y+b, z+c)$, where x, y, and z are integer values and a, b, and c are real values between 0 and 1, is approximated by standard trilinear interpolation from the eight surrounding grid points as follows [27]:

$$\begin{aligned} G(x+a,y+b,z+c) &= (1-a)(1-b)(1-c)G(x,y,z) + a(1-b)(1-c) \times G(x+1,y,z) + ab(1-c)G(x+1,y+1,z) \\ &\quad + abcG(x+1,y+1,z+1) + (1-a)b(1-c) \times G(x,y+1,z) + (1-a)bcG(x,y+1,z+1) \\ &\quad + a(1-b)cG(x+1,y,z+1) + (1-a)(1-b) \times cG(x,y,z+1) \end{aligned} \quad (2)$$

Since the DT values increase towards the interior of the object, the gradient vectors always point towards the center, starting orthogonally to the boundary surface. One can observe that the vector magnitude is smaller at the medial curve than all other points (see Fig. 1(b)).

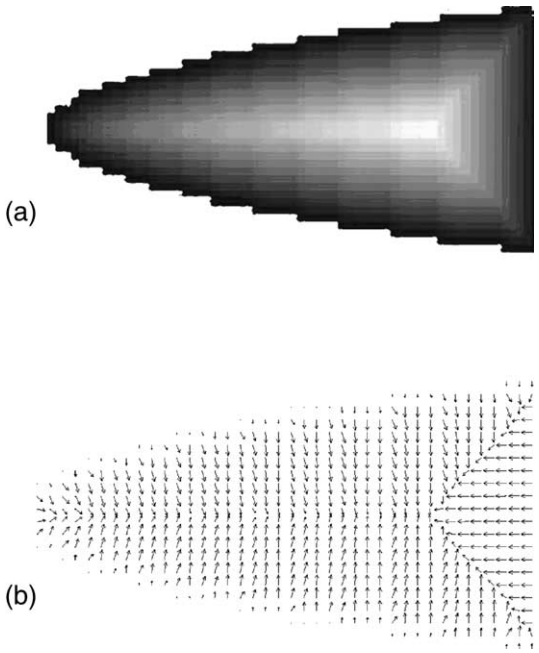

Fig. 1. (a) The distance transform map from the boundary. (b) The computed gradient field [6].

2.3. Initial path construction

With a voxel selected as the SP of the paths as described in Section 2.1, the end-points of the branches should be identified. The points which belong to the surface of the object and have the local maximum distance from SP, are defined as the end-points [17]. To this end, we need to compute the DT map from the reference point, SP, only for the voxels belonging to the surface. This DT-coded surface can be used for initial path construction. Computing the Euclidean distance map, one can obtain the exact distance. In this work, we have utilized an approximation to the Euclidean DT, which is Chamfer DT with ⟨3,4,5⟩ metrics for its exclusive merits [18,28]. The DT map is computed by assigning the SP voxel a distance of zero and iteratively assigning values to the neighboring voxels using weighted metrics: 3 for face, 4 for edge, and 5 for vertex neighbors.

Having the surface of the object coded, the computed DT map is used to determine the voxels with the maximum DT values. Each voxel on the surface is examined and compared to its adjacent voxels to assess if it has the maximum code or not. In order to avoid spurious end-points, we define a Neighboring Window (NW) in which the selected end-point must have the local maximum DT value. While small values for NW lead to spurious endpoints, large values lead to consuming much time without improving the result. A compromise, therefore, should be made to determine the optimum value for the NW. By trying different values of n for the $n \times n \times n$ NW, for different vascular objects, we found the value of 7 (i.e. a $7 \times 7 \times 7$ window) optimal.

The end-points determined based on the maximum code might be a few voxels away from the central curves. These points must ideally be at the centerline of the object, hence, for improved accuracy, the endpoints can be shifted on the surface of the object, in the direction of the gradient field.

With the end-points and the SP determined, the initial paths can be generated on the surface, starting from each end-point and finishing at the SP. The first path or the main

branch is constructed by connecting the end-point with the maximum distance value to the selected SP by monotonically decreasing in the distance. For any point in the distance map, the set of all neighbors with lesser distance values can be determined and this yields several possibilities for traversing the distance map: steepest descent, median descent and shallowest descent [14]. We preferred the steepest descent method, since it connects the extreme points with the shortest one-voxel-wide (thin) path. For the rest of the end-points, if any, paths are constructed starting from each end-point and terminating when a voxel on the previous paths is reached. At the end of this stage, we have paths with the number of object branches along with their corresponding end-points and SP.

2.4. Path centering

In order to centralize the paths that were initially constrained to lie on the surface of the object, we utilized a variant of the snake model, proposed by Cuisenaire [15]. In this model, the initial paths are considered as snakes that must evolve to where the defined potential energy has its minimum value. The image potential energy is the distance map defined in Section 2.2. To move the snake, the force derived from the gradient field should be applied perpendicularly, as the parallel component would only modify the sampling of the snake and not its location. To remove the parallel component, the force applied to each voxel of the snake is defined as follows [15]:

$$\overrightarrow{F(v)} = \overrightarrow{G(v)} - \frac{\vec{v}\cdot\overrightarrow{G(v)}}{|v|^2}\vec{v} \tag{3}$$

where v is a voxel which belongs to the snake. The force to be applied to the voxel is denoted by F. Applying this force to each voxel, we drive the snake towards the center of the object. The algorithm for centering the initial path or snake in pseudo code is as follows:

Path-Centering Algorithm:

```
For n = 1 to number of initial paths
    Snake := initial path (n);
    While the Snake is not stabilized do
        For each voxel, v, belonging to the Snake:
            Compute F(v);
            v_new := v + wF(v);
            v := v_new;
        End
    End
CenteredPath(n) := Snake;
End
```

w is the weight for the applied force. To define when the snake is stabilized, one can consider different criteria; for instance, setting a limit for the number of iterations, setting a minimum threshold for the force value applied to each voxel or setting a minimum value for the total applied force to the snake. In our method, the centering algorithm ends when the total force magnitude for the snake is less than 1 or the number of iteration exceeds 100. Normally, the paths are centered in less than 15 iterations (see Fig. 2).

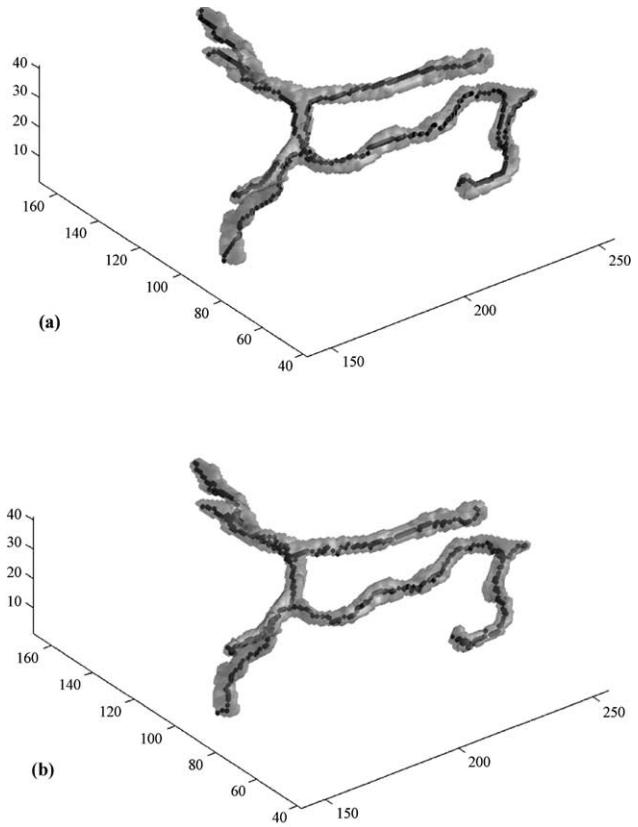

Fig. 2. (a) The initial paths on the surface. (b) The centered paths.

3. Algorithm improvements

3.1. Up and down sampling

In the process of path-centering using the snake model, the voxels generally may overlap with each other while moving towards the central region of the object or become separated giving rise to a non-connected centerline. Disconnectivity particularly occurs near the end-points of the branches where the gradient field is not zero. Overlapping and disconnectivity are both sources of error for the quantification of branches, such as length and diameter estimation, and must be avoided. Thus, we apply an up and down sampling on the centralized paths. Moving on each path, redundant voxels are removed, while additional voxels are inserted if two consecutive voxels are not neighbors.

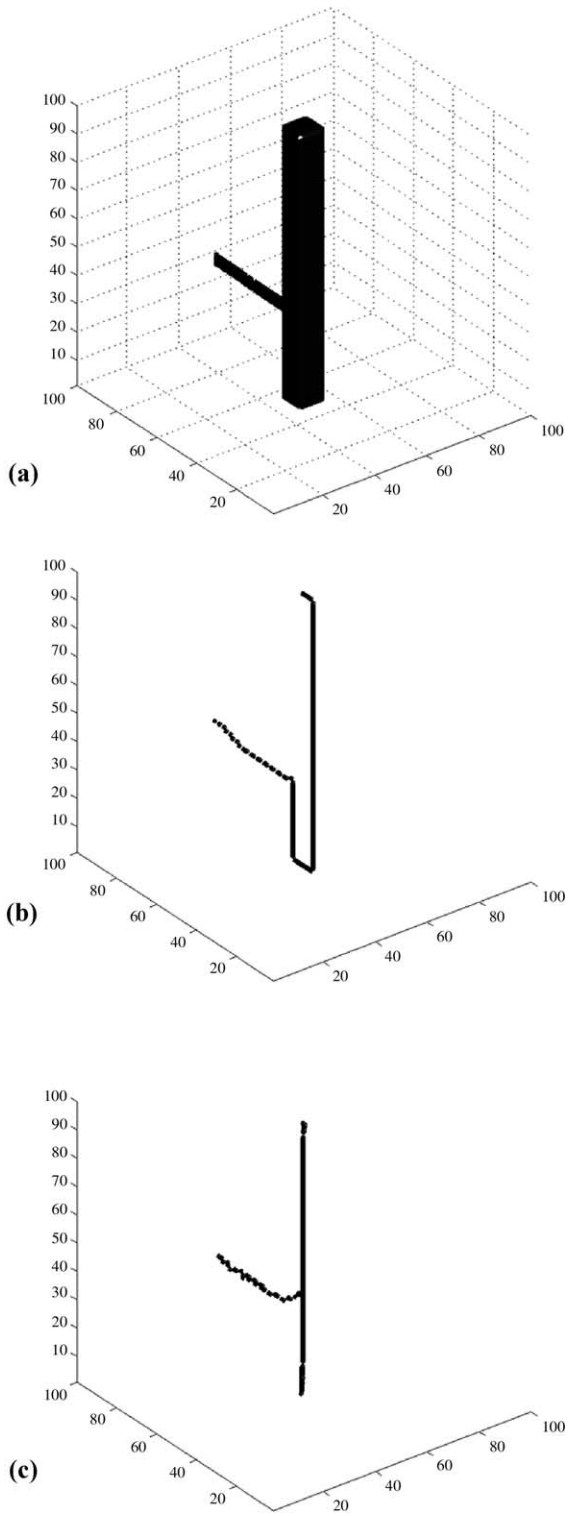

Fig. 3. (a) The simulated vessel. (b) The initial paths. (c) The extracted centerlines.

3.2. Updating the start points of branches

In the path-centering stage, some part of two initial paths which are converging to the central axis of the object, might overlap. This is not apparent when the centerlines of the object are illustrated. However, it results in a significant error when extracting quantitative parameters, since a part of the final centerline of the object is counted for more than one branch. To avoid this problem, a simple algorithm is developed to march on the final centerlines and update the SP of each branch. For any path and starting from an end-point, each voxels of the path is checked to assess if it belongs to the previous paths and if so, this voxel is set as the SP of the path.

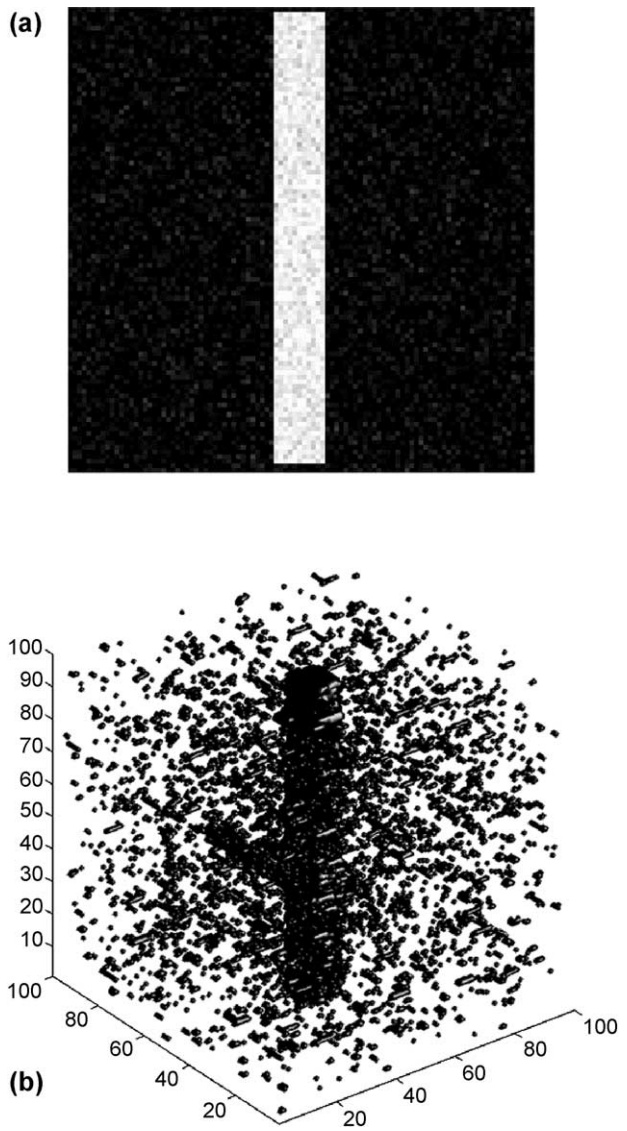

Fig. 4. (a) A noisy frame with NSD of 20. (b) The 3D visualization of the simulated object with NSD of 50.

4. Experimental results

The algorithm was implemented in MATLAB and was run on a Pentium III PC with 1000 MHz CPU with 256MB

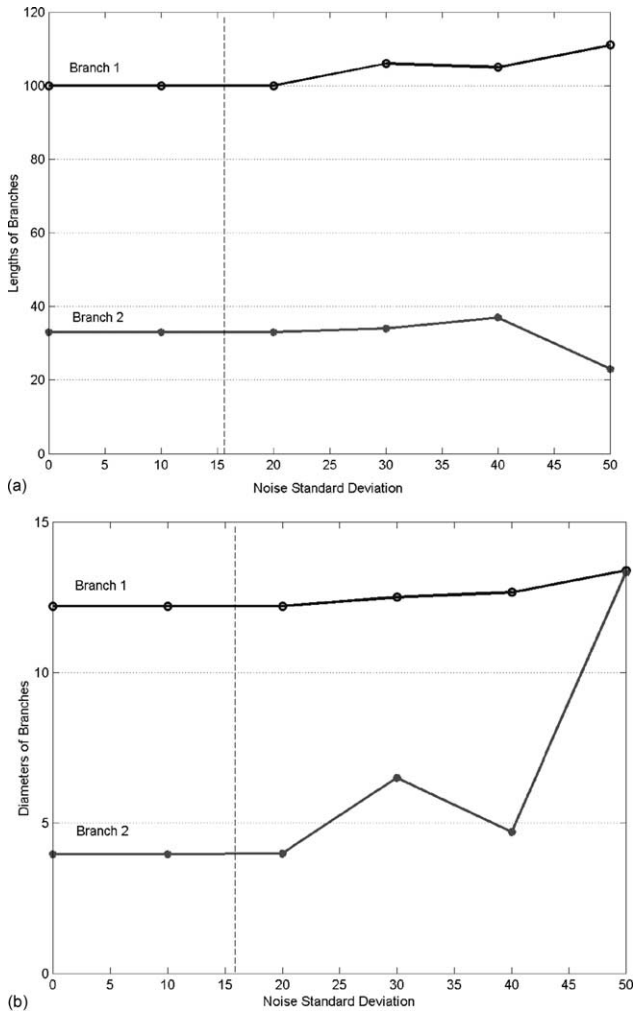

Fig. 5. The effect of noise on (a) the computed lengths and (b) diameters of branches.

of RAM. The acquired gray-level images were bi-leveled using a global threshold selected by inspecting the vessels and background areas for a set of CM images. Median filtering was also utilized to efficiently remove the isolated islands and fill small holes due to imaging distortion and noise.

4.1. Synthetic objects

We applied the proposed algorithm on simulated objects. One shown in Fig. 3(a), is a simple 3D object. The initial paths on its surface and the extracted centerlines are illustrated in Fig. 3(b) and (c), respectively. During the path-centering stage, the initial paths converge to the central curves. As mentioned before, if the SP of branches are not updated, their lengths may be significantly overestimated. This case will certainly happen for the test image, shown in Fig. 3(a), as the initial paths are completely separated from each other except for the SP of the main branch.

Noise sensitivity. To evaluate the noise sensitivity of the proposed algorithm, we applied the algorithm to the simulated image and computed the lengths and diameters of the object in the presence of noise. The additive noise to our 256-level images, is the zero-mean Gaussian noise with a standard deviation ranging from 0 to 50. A 2D cross-section of the noisy image with noise standard deviation (NSD) of 20 is shown in Fig. 4(a) and the 3D visualization of the simulated object with NSD of 50 is illustrated in Fig. 4(b). The lengths and diameters versus the NSD obtained by our method are shown in Fig. 5. Note that the typical NSD derived for our CM datasets is about 15.3 where the algorithm is immune to noise.

Table 1
The extracted features for normal and ischemia CM datasets

Dataset	Number of vessels		Total length (μm)		Vessel volume/tissue	
	Capillary	Pre-capillary	Capillary	Pre-capillary	Capillary	Pre-capillary
Normal						
1	105	0	6125.80	0.00	0.0840	0.0000
2	148	1	7349.60	55.58	0.0863	0.0008
3	83	0	5367.30	0.00	0.0493	0.0000
4	96	0	5765.00	0.00	0.0478	0.0000
5	83	1	5867.50	14.17	0.0489	0.0008
Average	103	0.4	6095.0	13.95	0.0633	0.0003
Ischemia						
1	105	4	3621.40	307.32	0.0266	0.0137
2	124	4	4053.00	239.76	0.0330	0.0096
3	194	2	5871.80	65.39	0.0674	0.0039
Average	141	3.33	4515.4	204.16	0.0423	0.0091

4.2. Real medical data

Eight CM datasets of vascular images of rat brains were used to test the algorithm (Table 1). The main advantage of the confocal, laser-scanning microscope is that it allows researchers to observe an object in three-dimensions and to gather quantitative data such as thickness, area, and volume of a cellular structure. Most confocal microscopes are computer-driven with a precision-made electronic step motor attached to the microscope stage. Computer commands move the stage up and down under the control of the step motor in increments smaller than 1 μm [29]. One can focus precisely up and down through a specimen, while looking at the computer monitor, by using computer commands rather than focusing controls on the microscope. A clear fully focused fluorescent image is achieved every step of the way. This allows one to collect any number of optical sections through the specimen [29].

The ability of CM imaging to section non-invasively allows one to collect a uniform series of optical sections, through the material at steps of 0.6 μm, which is the resolution limit of an optical microscope in the *Z*-direction [29]. For the purpose of visualization or quantification, these sections are to be processed in 3D.

The sections we used were analyzed with a Bio-Rad MRC 1024 (argon and krypton) laser scanning confocal imaging system mounted onto a Zeiss microscope (Bio-Rad; Cambridge, MA). The image size was $260.6 \times 260.6\ \mu m^2$ in the *X* and *Y* directions and 1 μm increment in the *Z*-direction.

Normal and stroke rat brains. A 3D visualization of a normal rat brain is illustrated in Fig. 6(b) where the complex structure of the vessels is obvious. The proposed method efficiently extracts the centerlines of the vessels as shown in Fig. 6(c). The centering stage takes less than 1 min and the extracted centerlines are thin, connected and accurately centered. In Fig. 7(a), a stroke rat brain is illustrated where the stasis of the vessels is detectable compared to the 3D image of a normal vascular dataset. The extracted centerlines for this $256 \times 256 \times 30$ dataset is shown in Fig. 7(b). In Table 1, some extracted features for normal and stroke rat brains are compared.

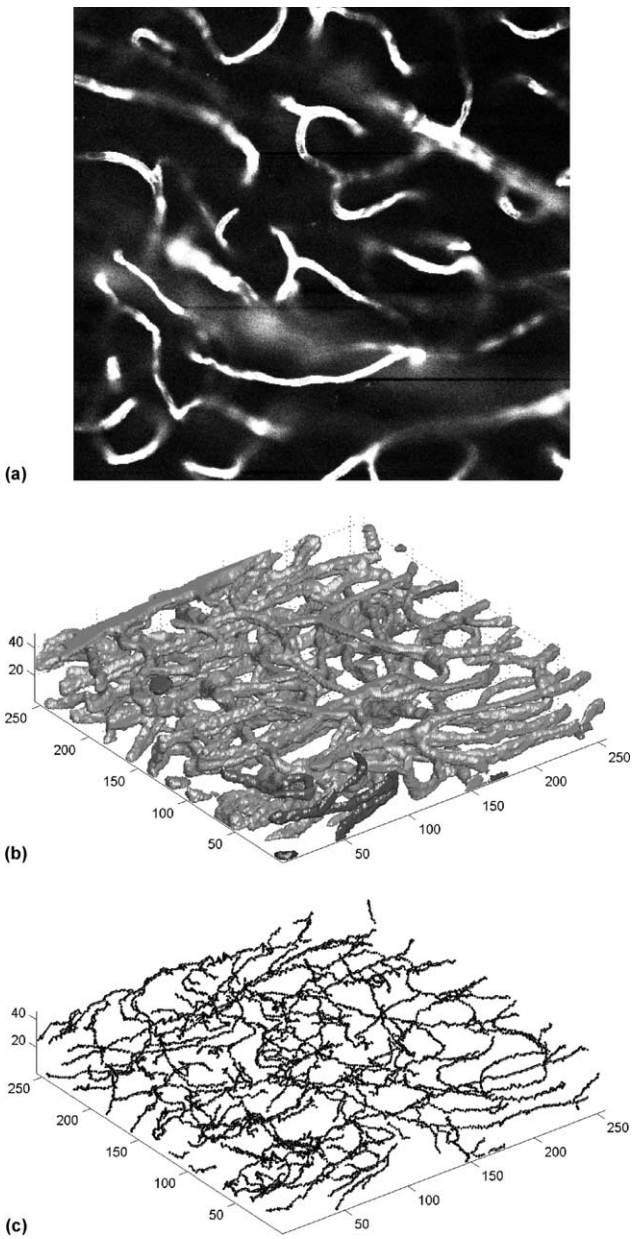

Fig. 6. (a) A 2D CM image. (b) The 3D visualization of a normal rat brain. (c) The extracted centerlines.

4.3. Comparison to previous work

A well-known centerline extraction technique is skeletonization and particularly the definition of the medial axis function of Blum [2]. However, if one wishes to have smooth and centered curves [30], he will need to rely on the results of post-processing techniques in order to obtain a unique and smooth path inside the segmented object [31]. Thinning methods also require further processing to smooth and remove undesirable small parts of the skeleton and moreover to distinguish its different branches.

In our approach, however, we extract accurate centered paths in a unique and fast process. Unlike the extracted skeletons by thinning methods, it contains no false or missing branches. Furthermore, each branch in the skeleton is distinguishable and so their lengths can be easily computed.

Herein, it is worth mentioning that the centerlines of structures which have loops are partially extracted. This is because the end-point is defined as the voxel with the maximum distance from the RP. For a loop, only one voxel is found as the end-point (which has the maximum DT value in the map). Thus, by traversing the steepest descent path, only the centerline for one half of the loop is extracted. Nevertheless, the purpose of our method is to have

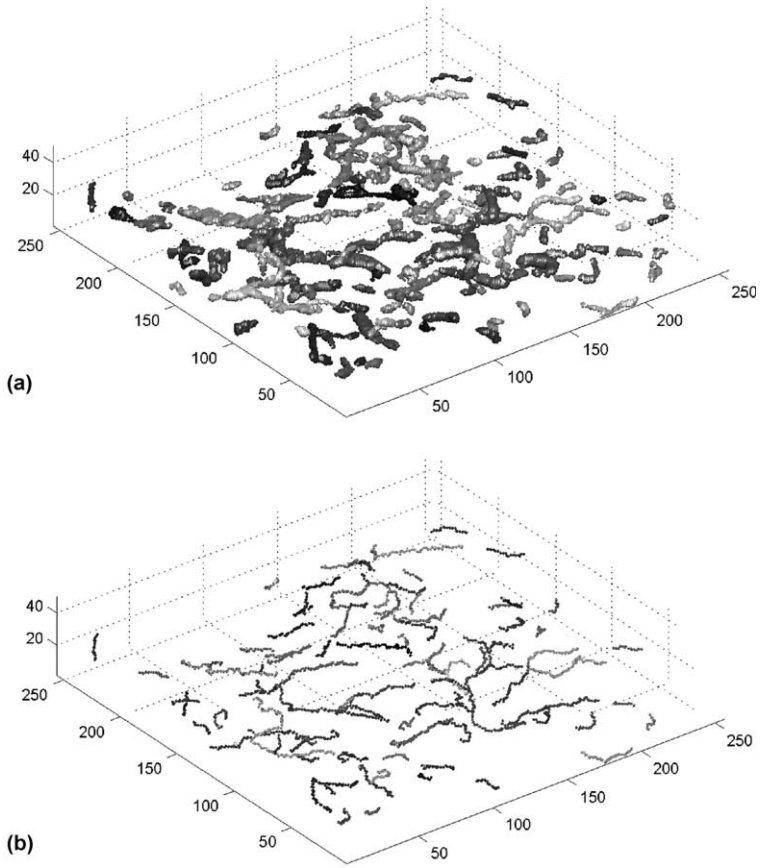

Fig. 7. (a) The 3D visualization of a stroke rat brain. (b) The extracted centerlines.

centerlines of vascular images, which are tree-like structures. In addition, the pre-processing stages remove most of the unreal loops.

Zhou and Toga [4] presented a DT-based method for skeletonization of volumetric objects. They have used two distance maps to approximate the distance of the object voxels from boundary voxels and a single RP. The use of recursive algorithms has made their skeletonization method time-consuming. In another DT-based algorithm reported by Shahrokni et al. [5], the recursive steps are bypassed, but it still takes a long time to analyze a set of complete confocal microscopic images. Compared with their approach, our proposed algorithm is computationally more efficient and is about 50% faster. In addition, the resulting centerline has no disconnectivity in the branch joints. The results of applying the thinning method of Ref. [32] and DT-based method of Ref. [5] on a single branching vessel are compared with our approach in Fig. 8. The medial curve obtained by the thinning method [32] has many spurious branches. The result of the DT-based method [5] is thin and without any extra or missing branches but is not connected. In Fig. 8(d), the centerline of the vessel is shown which has been obtained by using the snake model as described in this paper. This thin and connected centerline has been extracted in about half of the processing time needed for the path planning approach.

In another approach [1], a tracking process is presented to obtain a set of centerline points. The tracking is an iterative process in which an ordered set of points is computed step by step in a local area around the previous point [1]. A drawback of this method is that the initial point and the initial direction must be given. Although the method is very accurate, it fails for structures with branch angels of 10° or less and 170° or more [1].

Paik et al. [14] define the initial path on the surface of the colon and then move this path to the center of the object by applying a thinning algorithm to the object and projecting the path on the resulting surface. In our previous work [18], we extended and automated this method to be applicable for centerline extraction of complex vascular structures. Although, it produces smooth centered curves, the thinning algorithm is computationally inefficient, compared to the algorithm presented here, in which the centering stage is accomplished in a few seconds.

In another approach, Cuisenaire [15] first extracts the shortest path between the two given points and then centralizes it by a simplified active contour model concept which was first introduced by Kass [26]. We invoked his idea of using snake model for our centering step to move the paths, initially laid on the surface of the vessels. Deschamps and Cohen [16] presented a similar approach in which the 3D minimal paths are first obtained and then centralized by

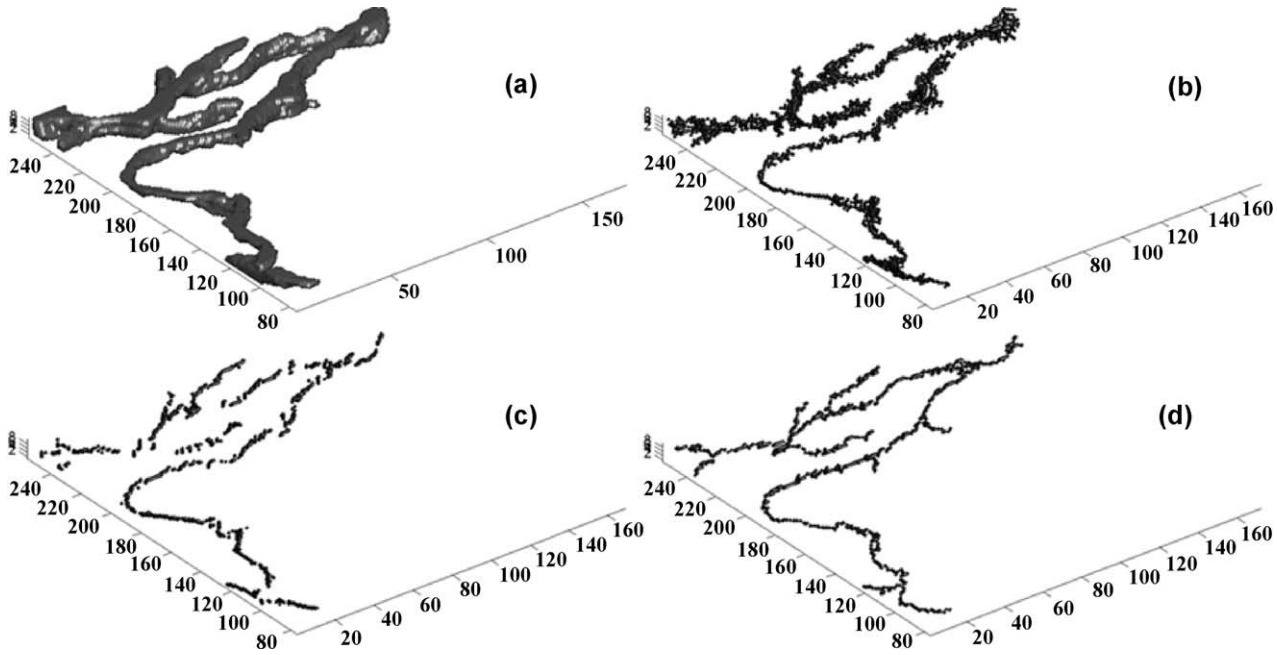

Fig. 8. (a) A single branching vessel; the extracted centerline obtained by (b) Thinning method [32]; (c) DT-based method [5]; (d) the proposed snake model. It can be observed that thinning method without any additional processing leads to a skeleton with many spurious branches and the DT-based method results in a disconnected curves, though it consume much time. However, our proposed method is about 60% faster and extract the thin and connected centerlines automatically.

minimizing a defined potential energy. The main feature of our method compared to the above mentioned works, lies in the fact that the proposed approach is totally automated and needs no user interaction to select points on the vessels. Furthermore, it is computationally less extensive, because it requires less DT mapping. Contrary to the methods proposed by Shahrokni [5], Cuisenaire [15] and Deschamps [16], where two different DT are computed for all the voxels of the object, our algorithm makes use of one DT for the whole voxels of the object and another one only for the voxels on the surface of the object.

5. Summary

A fast and efficient method for fully automated and accurate centerline extraction of elongated objects is presented. The proposed method is based on the DT concept, path planning, and active contour models. It generates thin and connected centerlines of objects without requiring any user interaction or any prior knowledge of the object shape. This automated method has been applied to the complex branching structures of the vascular images of rat brains generated by CM. The experimental results on both simulated and real medical images illustrated the efficiency of the method in extracting 3D centerlines of complex structures such as those in microvascular images.

The quantitative results from analyzing CM images of the normal and stroke rat brains illustrate that the proposed methods are sensitive to the differences between the two groups based on the number, total length, and relative volumes of both capillaries and pre-capillaries (see Table 1). These differences could not be evaluated without our methods and software. Important applications of the methods presented in this paper include evaluation of treatment responses in development of new drugs.

Acknowledgements

The authors would like to thank Dr Zhen G. Zhang of Henry Ford Health System for providing CM images and biomedical advice and Ali Shahrokni for his kind assistance.

References

[1] Flasque N, Desvignes M, Constans JM, Revenu M. Acquisition, segmentation and tracking of the cerebral vascular tree on 3D magnetic resonance angiography images. Med Image Anal 2001;5(3):173–83.
[2] Blum H. A transformation for extracting new descriptors of shape. In: Wathen-Dunn W, editor. Models for the perception of speech and visual form. Cambridge, MA: The MIT Press; 1967. p. 362–80.
[3] Gagvani N, Silver D. Parameter-controlled volume thinning. Graph Models Image Process 1999;61(3):149–64.
[4] Zhou Y, Toga AW. Efficient skeletonization of volumetric objects. IEEE Trans Visual Comput Graph 1999;5(3):196–209.
[5] Shahrokni A, Zoroofi RA, Soltanian-Zadeh H. A fast skeletonization algorithm for 3D elgonated objects. Proc SPIE Med Imaging Conf, CA 2001;4322:323–30.

[6] Schirmacher H. Extracting graphs from three dimensional neuron datasets. Diploma Thesis, Universite Erlangen-Nürnberg, 1998. Available at http://www.mpi-sb.mpg.de/~htschirm/publ/
[7] Ge Y, Fitzpatrick JM. On the generation of skeletons from discrete Euclidean distance maps. IEEE Trans Pattern Anal Mach Intell 1996; 18(11):1055–66.
[8] Palagyi K. A 3-subiteration 3D thinning algorithm for extracting medial surfaces. Pattern Recognit Lett 2002;23(6):663–75.
[9] Romero L Ros, Thomas F. Fast skeletonization of spatially encoded objects. Proceedings of 15th International Conference on Pattern Recognition, vol. 3. Los Alamitos, CA, USA: IEEE Computer Society; 2000. p. 510–3.
[10] Borgefors G, Nystrom I, Sanniti di Baja G. Computing skeletons in three dimentions. Pattern Recognit 1999;32(7):1225–36.
[11] Min Ma C, Sonka M. A fully parallel 3D thinning algorithm and its applications. Comput Vision Comput Graph 1996;5(3):420–33.
[12] Weian D, Lyengar SS, Brener NE. Order independent homotopic thinning for binary and gray tone anchored skeletons. Pattern Recognit Lett 2002;23(6):663–75.
[13] Nystrom I, Sanniti di Baja G, Svensson S. Curve skeletonization by junction detection in surface skeletons. Fourth Workshop on Visual Form, IWVF4, Proceedings; 2001. p. 229–38.
[14] Paik DS, Beaulieu CF, Jeffrey RB, Rubin GD, Napel S. Automated flight path planning for virtual endoscopy. Med Phys 1998;25(5): 629–37.
[15] Cuisenaire O. Distance transformations: fast algorithm and applications to medical image processing. PhD Thesis, Universite Catholique de Louvain, Belgium, 1999
[16] Deschamps T, Cohen LD. Fast extraction of minimal paths in 3D images and applications to virtual endoscopy. Med Image Anal 2001; 5(4):281–99.
[17] Maddah M, Afzali-Kusha A, Soltanian-Zadeh H. Fast centerline extraction of vessels in confocal microscopy images. Proceedings of IEEE International Symposium on Biomedical Imaging, Washington, DC; 2002. p. 461–4.
[18] Maddah M, Afzali-Kusha A, Soltanian-Zadeh H. Efficient center-line extraction for quantification of vessels in confocal microscopy images. Med Phys 2003;30(2):204–11. February.
[19] Cohen L, Kimmel R. Global minimum for active contours models: a minimal path approach. Ceremade 1996;TR9612.
[20] Sato Y, Nakajima S, Shiraga N, Atsumi H, Yushida S, Koller T, Gerig G, Kikinis R. Three dimensional multi-scale line filter for segmentation and visualization of curvilinear structures in medical images. Med Image Anal 1998;2(2):143–68.
[21] Krissian K, Malandain G, Ayache N, Vaillant R, Trousset Y. Model-based detection of tubular structures in 3D images. Comput Vision Image Understand 2000;80:130–71.
[22] Wilson DL, Noble JA. Segmentation of cerebral vessels and aneurysms from MR angiography data. Int Conf Image Process Med Imaging 1997;423–8.
[23] Chatzis V, Pitas I. A generalized fuzzy mathematical morphology and its application in robust 2-D and 3-D object representation. IEEE Trans Image Process 2000;9(10):1798–810.
[24] Datta A, Parui SK, Chaudhuri BB. Skeletonization by a topology-adaptive self-organizing neural network. Pattern Recognit 2001;34: 617–29.
[25] Chuang JH, Tsai CH, Ko MC. Skeletonisation of three-dimensional object using generalized potential field. IEEE Trans Pattern Anal Mach Intell 2000;22(11):1241–51.
[26] Kass M, Witkin A, Terzopoulos D. Snakes: active contour models. Int J Comput Vision 1987;321–31.
[27] Pratt WK. Digital image processing, 3rd ed. New York: Wiley; 2001.
[28] Svensson S, Borgefors G. Distance transforms in 3D using four different weights. Pattern Recognit Lett 2002;23:1407–18. July.
[29] Rowland RE, Nickless EM. Confocal microscopy opens the door to 3-dimensional analysis of cells. Biosciene 2000;26(3):3–7.
[30] Yeorong G, Stelts DR, Jie W, Vining DJ. Computing the centerline of a colon: a robust and efficient method based on 3D skeletons. J Comput-Assist Tomography 1999;23(5):786–94.
[31] Tek H, Kimia B. Boundary smoothing via symmetry transforms. J Math Imaging Vision 2001;14(3):211–3.
[32] Maddah M, Afzali-Kusha A, Soltanian-Zadeh H. A fast thinning method for 3D skeletonization. Third Student Conference on Biomedical Engineering, Tehran, 8–10 May; 2002.

Mahnaz Maddah was born in Tehran, Iran, in 1978. She received her BSc and MSc degrees in electrical engineering: electronics from the University of Tehran, Tehran, Iran, in 2000 and 2002, respectively. In 2001, she joined the Signal and Image Processing Group at the Institute for Theoretical Physics and Mathematics, Tehran, Iran, where she is currently a researcher. Her research interest is image processing and computer vision.

Hamid Soltanian-Zadeh was born in Yazd, Iran in 1960. He received BSc and MSc degrees in electrical engineering: electronics from the University of Tehran, Tehran, Iran in 1986 and MSE and PhD degrees in electrical engineering: systems and bioelectrical science from the University of Michigan, Ann Arbor, Michigan, USA, in 1990 and 1992, respectively. From 1985 to 1986, he was with the Iran Telecommunication Research Center, Tehran, Iran. In 1987 he was a lecturer of electrical engineering at the University of Tehran, Tehran, Iran. Since 1988, he has been with the Department of Radiology, Henry Ford Health System, Detroit, Michigan, USA, where he is currently a Senior Staff Scientist. Since 1994, he has been with the Department of Electrical and Computer Engineering, the University of Tehran, Tehran, Iran, where he is currently an Associate Professor. Dr Soltanian-Zadeh's research interests include medical imaging, signal and image reconstruction, processing, and analysis, pattern recognition, and neural networks.

Ali Afzali-Kusha was born in Tehran, Iran, in 1966. He obtained a BSc degree from the Sahrif University of Technology, Tehran, Iran, in 1988, a MSc degree from the University of Pittsburgh, Pittsburgh, PA, USA, in 1991, and a PhD degree from the University of Michigan, Ann Arbor, MI, USA, in 1994, all in electrical engineering. Since 1995, he has been with the Department of Electrical and Computer Engineering, the University of Tehran, Tehran, Iran, where he is currently an Associate Professor. Dr Afzali-Kusha has been a research fellow at the University of Michigan, Ann Arbor, MI, USA, from 1994 to 1995, at the University of Toronto, Toronto, Ont., Canada, in 1998, and at the University of Waterloo, Waterloo, Ont., Canada, in 1999. His area of research includes medical imaging and analysis, laser tissue interaction, and electronics.